Supporting Information

Basu et al. 10.1073/pnas.1704372114

C. elegans Strain Genotypes

We used the following single mutants: *dlk-1(tm4024) I*, *pmk-3 (ok169) IV*, *ebp-1(tm1357) V*, *let-7 (mg279) X*, *let-7(n2853ts) X*, *daf-2 (e1370) III*, *efa-6 (ok3533) IV*, *slt-1 (eh15) X*, *atfs-1 (gk3094) V*, *vab-19 (e1036) II*, *ced-7(n1996) III*, *eff-1 (ok1021) II*, *lin-41(ma104) I*, *psr-1(tm469) IV*. Following are the double mutants used: *ced-7 (n1996) III*; *let-7(mg279) X*, *eff-1 (ok1021) II*; *let-7(mg279) X*; and *lin-41(ma104) I* ; *let-7(mg279) X*. The extrachromosomal DNA-containing strains used were *let-7 (mg279)*; *shrEx11* (P*mec-4-let-7*), *let-7(mg279)*; *shrEx12* (P*mec-4-let-7*). Transgenes were introduced into *let-7* mutant backgrounds by crossing. Homozygosity for all mutations was confirmed by either PCR or sequencing. We used the following published transgenes: P*mec-7*-GFP (*muIs32*), P*mec-4*-GFP (*zdIs5*), and P*mec-7*-GFP::RAB3 (*jsIs821*) (40). The *tbIs222* transgene was generated by the integration of extrachromosomal array *vdEx263* [P*mec-4*-mCherry (5 ng/μL) + P*odr-1*-dsRed (30 ng/μL)] described earlier (55). It was integrated by the TMP/UV integration procedure. The strains carrying newly generated extrachromosomal transgenes are described in Table S4.

Correlation of Quantitative Functional Recovery with Axon-Fusion Events at the Level of a Single Worm

The mean PTRI of the left or right side of worms that had undergone mock axotomy (a laser shot ∼6 μm away from the axon) was used as $PTRI^{preaxotomy}$. After axotomy, PTRIs of each side of the worms (left and right PLM) were measured at 3 h (for bead-immobilized worms) or 10 h (for worms immobilized with anesthesia) and were denoted as the $PTRI^{postaxotomy}$ of a particular side of a given worm. Each worm was labeled and kept in single plate at 20 °C. After 24 h, PTRI values ($PTRI^{24h}$) of both sides of the same worm were measured and compared with the corresponding values at the postaxotomy stages. For each worm, delta loss (ΔL) ($PTRI^{preaxotomy} - PTRI^{postaxotomy}$) and delta gain (ΔG) ($PTRI^{24h} - PTRI^{postaxotomy}$) values were obtained for the left or right side. For a given side of a particular worm, the FR was obtained by the following formula: FR = ΔG ($PTRI^{24h} - PTRI^{postaxotomy}$)/ΔL ($PTRI^{preaxotomy} - PTRI^{postaxotomy}$). Immediately after the behavioral test at 24 h, the regrowth phenotypes (fusion or nonfusion event) of the PLMs on each side were visualized and scored using a Leica DM5000 B fluorescent microscope at 40× magnification. The representative images of the regrowth phenotypes were imaged using a 63× oil lens (NA 1.46) Zeiss LSM 510 Meta Point Scanning confocal microscope with LSM 510 software. Therefore, for a particular side of a worm, the FR value could be correlated with the regeneration event (fusion or nonfusion) of the PLM on that side.

Axotomy and Functional Recovery Experiment in *let-7(n2853)* Worms

Both the wild-type control and *let-7 (n2843ts)* strains were grown at the permissive temperature of 15 °C. Axotomy was performed in a microscopy room, which is maintained at 20 °C. Immediately after axotomy, both control and *let-7 (n2843ts)* worms were divided into two batches. One batch was kept at the permissive temperature of 15 °C and the other at nonpermissive temperature of 20 °C. Therefore, for both the backgrounds, the PTRI values and fusion rates were obtained during regeneration at these two temperatures. The gentle touch response assay and PTRI measurement were performed 3 and 24 h after axotomy.

Axotomy and Imaging of AVM

For axotomy of AVM neurons at the L4 stage, we first ablated PVM neurons at the L2 stage to decrease the GFP intensities in the ventral nerve cord so that the AVM axon could be identified easily. At the L4 stage, the worms were immobilized using 10 mM levamisole hydrochloride in a 5% agarose pad and then were rolled by applying a little sliding pressure on the coverslip, so that the AVM axon in the ventral side was visible. The AVM axon was cut at a distance of 60–70 μm from the cell body. Then at 24 h postaxotomy, for confocal imaging of the regeneration events, the worms were immobilized using same protocol used for axotomy. The regenerated AVM axon was imaged using the 63× oil lens (1.46 NA) of a Zeiss LSM 510 Meta confocal microscope with LSM 510 software.

Primers Used for qRT-PCR and Fold-Change Calculation

The following primers were used: for the *lin-41* gene: lin-41qF: 5′-TCAACACTGCCATCGCCGCC-3′, lin-41qR: 5′-TCCAAGCGAGACCAGGCTTCAG-3′ (54); for the *ced-7* gene: ced-7qF1: 5′-CCATCAATTCATATGCTGCTG-3′, ced-7qR1: 5′-GATTGCACAGAAGAGAGGAAT-3′, ced-7qF2: 5′-GAGGAAGCTGCTAATTTTGAG-3′, ced-7qR2: 5′-CATCTACAGTACCGGTTAGAC; for the *eff-1* gene: eff-1qF1: 5′-GATCTTGTTGAGGGAAAATGG-3′, eff-1qR1: 5′-CAAAACTCCGAGATACACAAC-3′, eff-1qF2: 5′-CTGCAAATCATTATATGCCAGG-3′, eff-1qR2: 5′-GATGATGGATCCACTGAAGTC-3′; for the *psr-1* gene: psr-1qF: 5′-GCTCTGTCGAGAATTTGCATC-3′, psr-1qR: 5′-CGTCAGATGATGAGGAAGAGC-3′; *tba-1* was used as the control gene: tba-1qF: 5′-TCAACACTGCCATCGCCGCC-3′, tba-1qR: 5′-TCCAAGCGAGACCAGGCTTCAG-3′ (54)

Fold change $2^{-\Delta\Delta Ct}$ calculation (34):

$$\Delta Ct \text{ target gene in wild type} = Ct \text{ target gene (wild type)} - Ct \textit{ tba}\text{-}1\text{(wild type)}$$

$$\Delta Ct \text{ target gene in } \textit{let}-7(n2853ts) = Ct \text{ target gene } [\textit{let}\text{-}7(n2853ts)] - Ct \textit{ tba}\text{-}1[\textit{let}\text{-}7(n2853)].$$

$$\Delta\Delta Ct \text{ of target gene} = \Delta Ct \text{ target gene in } \textit{let}\text{-}7(n2853ts) - \Delta Ct \text{ target gene in wild type. Fold change} = 2^{-\Delta\Delta Ct}$$

Experiments Related to Aging

Worms were age synchronized using 50 mM 5-fluoro-2′-deoxyuridine (FuDR ; Sigma F0503) in NGM plates. Approximately 50–60 gravid adults were transferred to a drop of sodium hypochlorite (bleach) solution on a seeded plate. After 2 d, ∼15–20 L4 worms were transferred to OP50-seeded FuDR plates and were grown in 20 °C. Plates were checked every 2–3 d for availability of OP50 food. If the food was exhausted, the worms were transferred to new FuDR plates. In this way, worms were aged. To make survival plots of different genotypes, after transfer at the L4 stage, the numbers of living and dead worms were counted each day. Living and dead worms were differentiated by their locomotion ability and other death-related phenotypes. The last day of the survival plot was the day when no live worms remained on the plate (56). A well-known long-lived mutant with a loss-of-function mutation in the insulin/IGF receptor *daf-2* was used.

Analysis of GFP::RAB3 Dynamics

Kymographs (Fig. 6 *C* and *D*) were generated using ImageJ software (https://imagej.nih.gov/ij/) from a 30-μm ROI placed on the PLM process (Fig. 6 *A*, *a′* and *b′*). The horizontal axis of the kymograph is the axon length in micrometers, and the vertical axis is the time in seconds. Typical GFP::RAB-3 tracks are displayed as diagonal lines (yellow traces for anterograde tracks and red traces for retrograde tracks in Fig. 6 *C*, *D*, *G*, and *H*). The ROI was drawn in the distal-to-proximal direction (toward cell body). From each kymograph, anterograde and retrograde particle movement [particle flux (41)] was quantified by calculating number of tracks in either the anterograde or retrograde direction per unit of length (in micrometers) and per unit of time (in seconds). The perpendicular tracks (white arrowheads in Fig. 6*D*) were considered to be particles that were static during the course of imaging. In many conditions, the fused (Fig. 6 *A*, *a′*) or regrowing (Fig. 6 *A*, *b′*) PLM axon remains in a single focal plane and can be fully imaged using spinning-disk microscopy. When the axon grew into multiple focal planes, GFP::RAB-3 dynamics could not be reliably imaged.

To reduce the background fluorescence of GFP::RAB-3 in the PLM axon, photobleaching was done on a 95-μm^2 ROI placed near the junction of a T2 fusion event (Fig. 6 *A*, *a′* and Movie S4*A*). Two hundred pulses were delivered from the 488-nm laser (pulse duration, 6 ms; laser power, 100%). Then time-lapse imaging of GFP::RAB-3 was done using the same imaging parameters.

Quantification of EFF-1:: mCherry Intensity

The intensities of EFF-1::mCherry and GFP from the specific ROIs (Fig. 6*G*) were measured using Image J software. For the baseline intensities before axotomy, the average intensities were measured in a 10-μm ROI placed on a PLM axon at a distance of 50 μm from the PLM cell body. The intensities of EFF-1::mCherry and GFP in the PLM at 30 min and 6 h postaxotomy were measured in two 10-μm ROIs, one drawn on the growing end (R-I) and other 10 μm away from the R-I toward cell body (R-II) (Fig. 6*G*). To measure the intensity in each ROI, the respective background was subtracted.

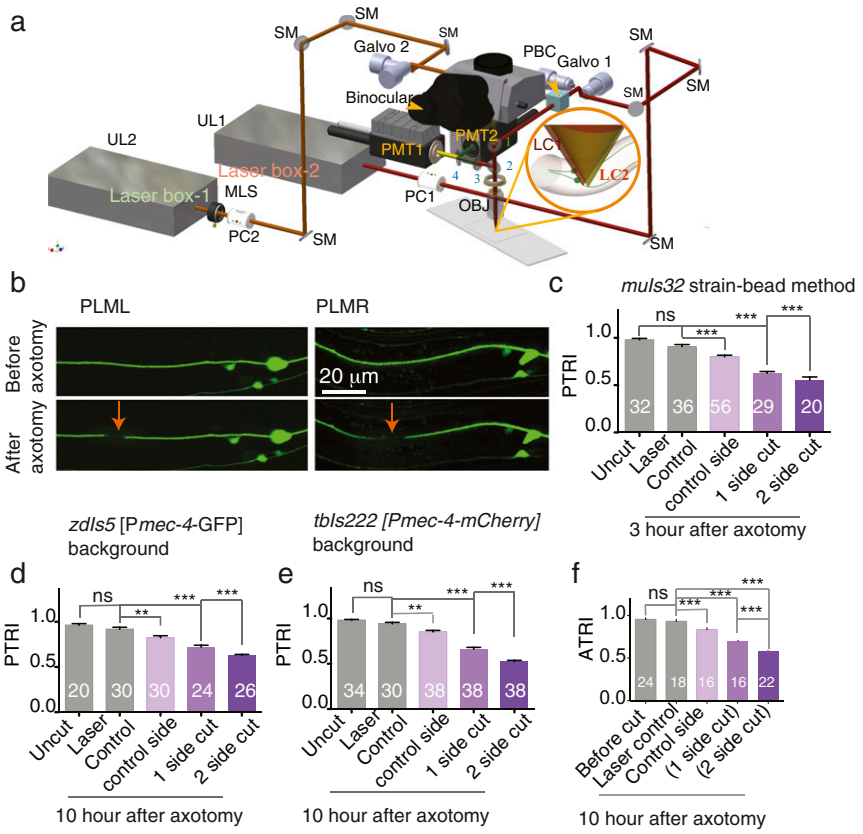

Fig. S1. A drop in the response index after axotomy using the femtosecond lasers of a two-photon microscope. (*A*) An optical ray diagram showing the light paths of the two lasers and the essential components of the imaging system. Galvo, galvanometer laser scanner; LC, laser cone; MLS, mechanical laser shutter; OBJ, objective; PBC, polarizing beam combiner; PC, pockel cell; PMT, GAsP photomultiplier tube; SM, silvered mirror; UL1&2, ultrafast lasers 1 and 2. (*Inset*) Position of the laser cones for imaging and axotomizing the PLM in the worm. (*B*) Representative images of PLM neurons on right and left side of a worm collected using two-photon imaging before and after axotomy at the L4 stage. Arrows indicate the position of the axotomy on the PLM neurons. The PLM neuron is expressing the transgene *muls32* (P*mec-7*-GFP). (Scale bar, 20 μm.) (*C*) Bar chart showing the PTRIs measured in worms before and 3 h after cutting PLM neurons. Here we used polystyrene beads to immobilize the worms. Cutting both PLMs has a stronger effect on the index than cutting one PLM. $N = 2$ independent replicates. (*D* and *E*) Bar charts show the PTRIs in worms labeled with *zdIs5* (P*mec-4*-GFP) ($N = 2$) (*D*) or *tbIs222* (P*mec-4*-mCherry) ($N = 2$ or 3) (*E*) before (Uncut) and after axotomy. (*F*) Axotomy of the ALM affects the ATRI. The ATRI was measured in worms before axotomy and at 10 h postaxotomy. ($N = 2$). In *C–F*, $^{**}P < 0.001$; $^{***}P < 0.0001$; ANOVA with Newman–Keuls multiple comparisons test. n = the number of sides tested for the touch assay. Error bars represent SEM. ns, not significant.

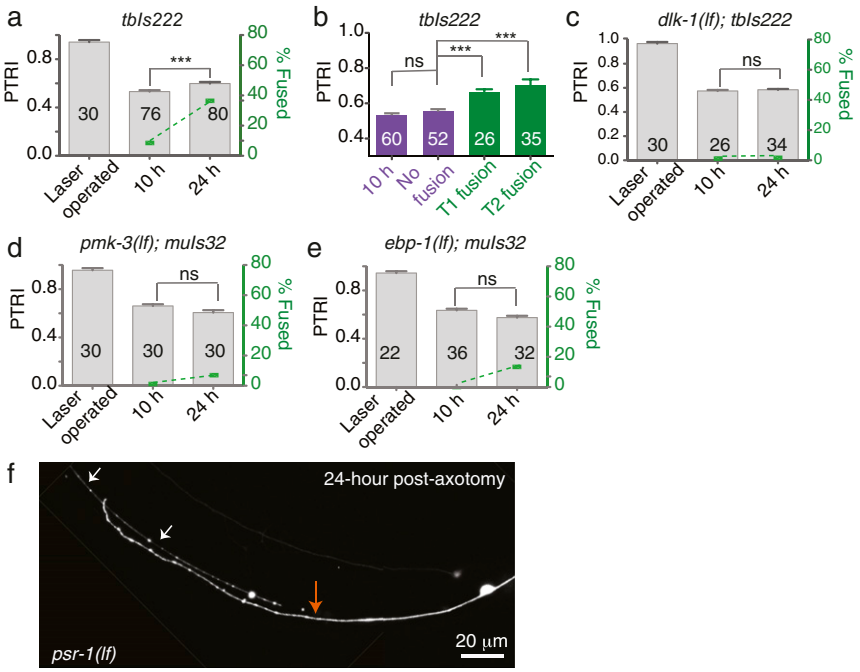

Fig. S2. Fusion between the proximal and distal fragments promotes functional recovery. (*A*) The bar chart shows a double *y*-axis plot for the PTRI (*Left*) and percent fusion (*Right*) in *tbIs222* (P*mec-4*-mcherry) worms at 10 and 24 h postaxotomy. There was a significant increase in PTRI and fusion events at 24 h compared with 10 h. $N = 2$–4 independent replicates. (*B*) Bar plot of the experiment in *A* separating the PTRI values in the nonfusion, T1 fusion, and T2 fusion categories. PTRI values are significantly higher in the fusion categories than in the nonfusion category. $N = 5$. (*C*) A double-axis plot as in *A* giving the PTRI and percent fusion values in *dlk-1(lf)* in the *tbIs222* background. There was no recovery in PTRI at 24 h after axotomy in *dlk-(lf)* worms. $N = 2$. (*D* and *E*) Similar double-axis plots for *pmk-3(lf)* (*D*) and *ebp-1(lf)* (*E*) mutants in the *muIs32* background. The PTRI value is not increased at 24 h in either of these mutants. For both *D* and *E*, $N = 2$. In *A*–*E*, $^{***}P < 0.0001$; ANOVA with Newman–Keuls multiple comparisons test. The number in each bar shows the number of sides tested. Error bars represent SEM. (*F*) A confocal image of a nonfusion event in a *psr-1(lf)* worm at 24 h after axotomy. The point of the axotomy is marked by an orange arrow; white arrows represent the degenerated distal end. ns, not significant.

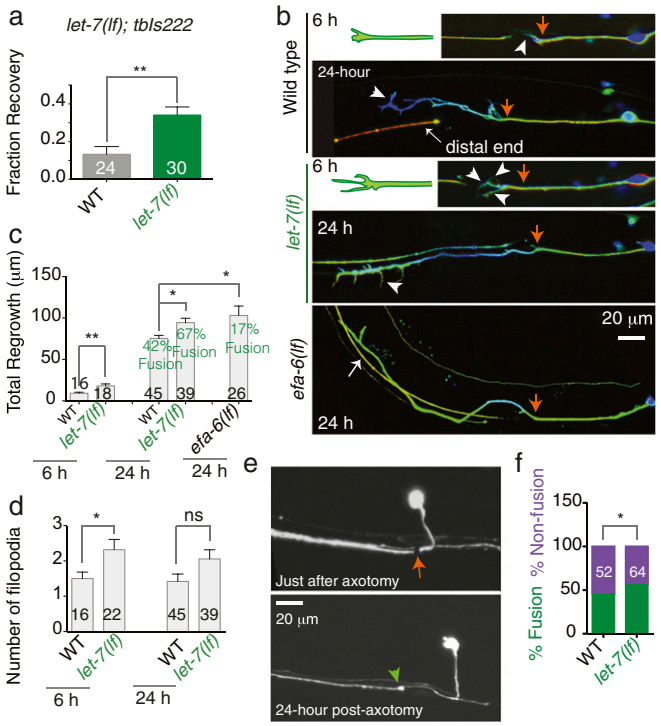

Fig. S3. *let-7* specifically inhibits axonal fusion. (*A*) The *let-7(lf)* mutant shows increased FR in the *tbIs222* (P*mec-4*-mCherry) background. $N = 2$ independent replicates. $^{**}P < 0.001$; unpaired *t* test with Welch's correction. (*B*) Representative confocal images of axon regrowth events classified as nonfusion in wild-type, *let-7(lf)*, and *efa-6(lf)* strains. To obtain a z-projected image, images from four focal planes were merged using a depth code with surface focal planes in red and deep planes in blue, thereby distinguishing the plane of the regrowing proximal end from the distal one. Orange arrows indicate the site of axotomy. At early time points of regrowth, the *let-7(lf)* mutant shows more sprouts or filopodia-like structures (white arrowheads). For 6-h total regrowth, $^{*}P < 0.01$; unpaired *t* test with Welch's correction. For 24-h total regrowth, $^{*}P < 0.01$; $^{**}P < 0.001$; ANOVA with Newman–Keuls multiple comparisons test. (*C*) Bar chart showing the quantification of total regrowth in the wild-type, *let-7(lf)*, *and efa-6(lf)* strains. (*D*) Bar chart showing the number of filopodia emerging from the cut tip in the wild-type and *let-7(lf)* strains 6 and 24 h postaxotomy. The *let-7(lf)* mutant showed significantly high numbers of filopodia/sprouts at 6 h postaxotomy. $^{*}P < 0.01$; unpaired *t* test with Welch's correction. $N = 1$–4 independent replicates. In both *C* and *D*, n = number of axons. (*E*) Confocal image of an AVM neuron immediately after axotomy and at 24 h postaxotomy. The orange arrow indicates the site of axotomy. At 24 h the proximal end (green arrowhead) has fused to the distal end. (*F*) Percentage of fusion events in the AVM neuron is increased in the *let-7(lf)* mutant. $^{*}P < 0.01$; unpaired *t* test with Welch's correction. $N = 3$; n = number of axons. Error bars represent SEM. ns, not significant.

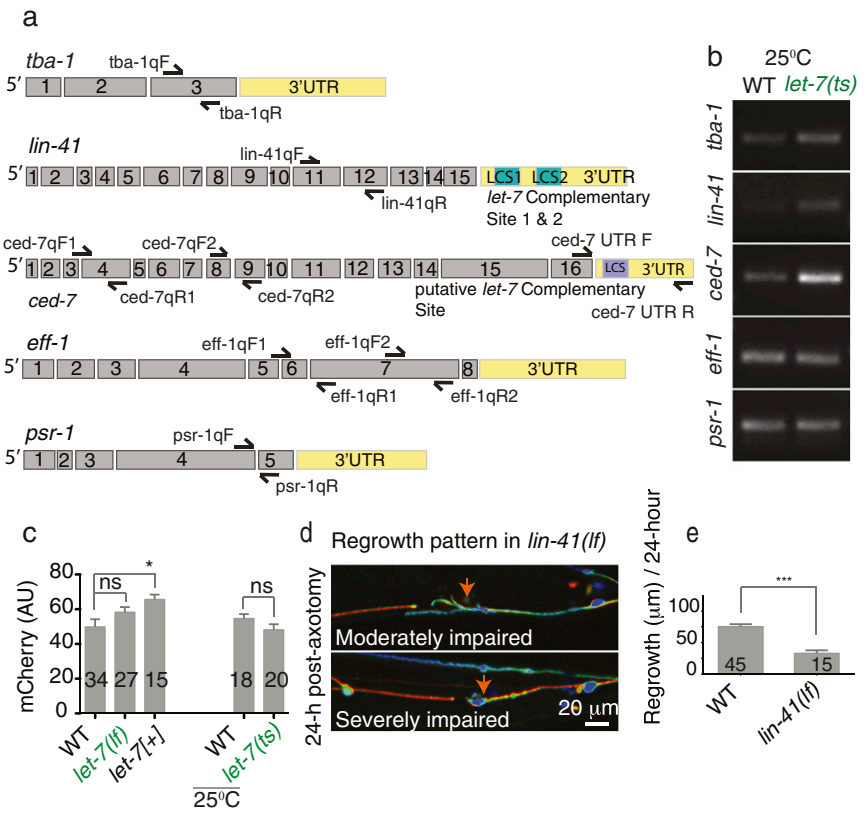

Fig. S4. Positions of the qRT-PCR primers. (*A*) Relative positions of the primers on different genes tested in the SYBR Green-based qRT-PCR reactions. Gray boxes represent exons. There are two *let-7* complementary sites, LCS1 and LCS2, in the 3′ UTR of *lin-41*, which is an established target of *let-7* miRNA. The 3′ UTR of *ced-7* has a sequence similar to LCS2. (*B*) The products of the qRT-PCR were run in a 3% agarose gel containing ethidium bromide and were visualized under UV. (*C*) Bars showing the average intensities of mCherry (internal control) expressed in worms along with the GFP reporter of the 3′ UTR of ced-7 as shown in Fig. 4*G*. mCherry intensity remains mostly unaffected in genetic backgrounds of varying doses of *let-7*. For *let-7(lf)*, *let-7(+)*, and relevant controls, $*P < 0.01$; ANOVA with Newman–Keuls multiple comparisons test; for the data involving the *let-7(n2853ts)* mutant, ns, not significant; unpaired *t* test with Welch's correction. $N = 2$–4 independent replicates. (*D*) Regrowth patterns in *lin-41(lf)* at 24 h postaxotomy. (*E*) Total regrowth in *lin-41(lf)* is significantly reduced at 24 h. $***P < 0.0001$; unpaired *t* test with Welch's correction; numbers in the bars represent the number of axons; $N = 2$. Error bars represent SEM.

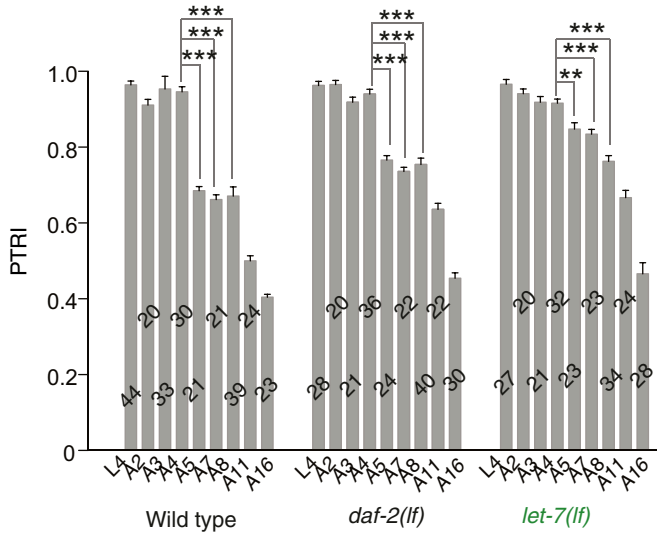

Fig. S5. Age-related decline of the PTRI. The bar plot presents the PTRI value in wild-type, *daf-2 (lf)*, and *let-7 (lf)* strains at different ages. In all three genotypes the PTRI decreases from the A5 stage. *n* = the number of sides tested. $N = 2$–4 independent replicates. $**P < 0.001$, $***P < 0.0001$; ANOVA with Newman–Keuls multiple comparisons test. Error bars represent SEM.

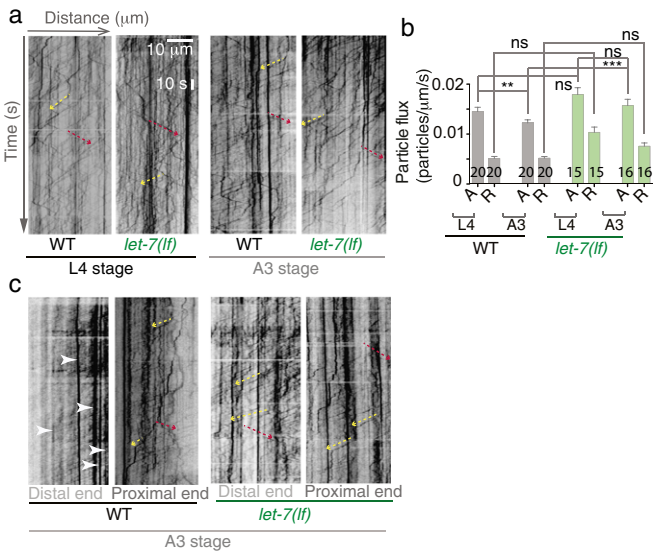

Fig. S6. The baseline axonal transport in control and *let-7(lf)* worms. (*A*) Representative kymographs obtained after time-lapse imaging of GFP::RAB-3 in the wild-type and *let-7(lf)* strain before axotomy at the L4 and A3 stages. Kymographs were obtained in a 30-μm ROI placed on the PLM axon at 10 μm from the cell body. Yellow arrows and red arrows trace movement events in the anterograde and retrograde directions, respectively. (Scale bars: 10 μm in the *x* axis and 10 s in the *y* axis of the kymographs.) (*B*) The bar chart represents the GFP::RAB-3 particle flux in the given ROIs in the wild-type and *let-7(lf)* strains. ***$P < 0.0001$; **$P < 0.001$; ns, not significant; ANOVA with Newman–Keuls multiple comparisons test. Error bars represent SEM. $N = 2$–4 independent replicates. A, anterograde; R, retrograde. (*C*) Representative kymographs of fused axons at 24 h postaxotomy in the wild-type and *let-7(lf)* strains at the A3 stage (Fig. 6*F*).

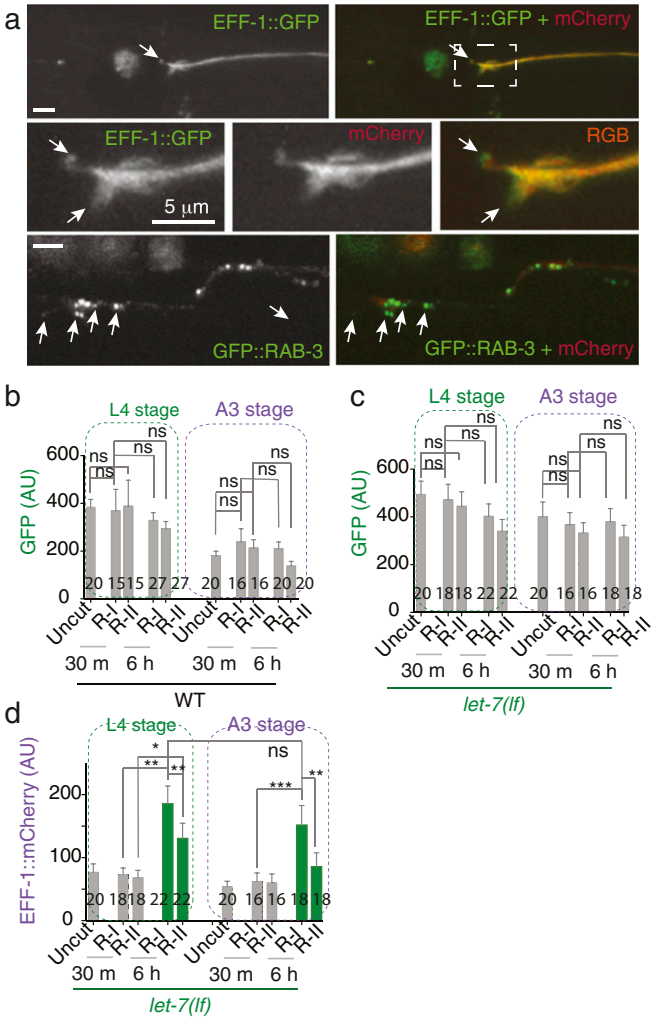

Fig. S7. Localization of EFF-1 at the growth cone tip. (*A*, *Top Row*) The growing end of a PLM expressing *shrEx58* (P*mec-4*-EFF-1::GFP) and *tbIs222* (P*mec-4*-mCherry) was imaged using point-scanning confocal microscopy at 6 h postaxotomy. mCherry is shown in red, and EFF-1::GFP is shown in green. White arrows indicate enrichment of EFF-1::GFP at the tip of filopodia. (*Middle Row*) An enlarged view of the growth cone shown within the dashed box in the upper row. (*Bottom Row*) The growth cone region of the PLM expressing *jsIs821* (P*mec-7*-GFP::RAB-3) and *tbIs222* (P*mec-4*-mCherry). GFP::Rab-3 puncta are also accumulated at the growth cone. (Scale bar: 5 μm.) (*B* and *C*) The average intensity of diffusible GFP in two ROIs, shown in Fig. 6*G* (R-I near the cut tip and R-II 10 μm away from R-I), obtained before axotomy and at 30 min and 6 h postaxotomy. The average intensity of GFP did not increase after axotomy in any of the ROIs in the wild-type (*B*) or *let-7(lf)* (*C*) strain. *n* = number of axons. (*D*) Average intensity of EFF-1::mCherry in the two ROIs described in Fig. 6*G* in the *let-7(lf)* strain obtained before axotomy and at 30 min and 6 h postaxotomy; *N* = 2–4 independent replicates. In *B–D*, $*P < 0.01$, $**P < 0.001$; $***P < 0.0001$; ANOVA with Newman–Keuls multiple comparisons test. Error bars represent SEM. ns, not significant.

Table S1. Values of fusion percentage in different mutants

Background	Allele	% fusion	Axons fused	Axons nonfused	Total no. axons
muIs32 (P*mec-7*-GFP)	Wild type	42	142	198	340
	let-7(mg279)	67	167	83	250
	let-7(n2853ts) @20 °C	68	40	20	60
	let-7(n2853ts) @15 °C	28	18	46	64
	daf-2(e1370)	27	28	76	104
	efa-6(ok3533)	17	19	89	108
	slt-1(eh15)	46	45	53	98
	atfs-1(gk3094)	12	9	63	72
	vab-19(e1036)	25	23	69	92
	ced-7(n1996)	24	35	109	144
	eff-1(ok1021)	10	14	130	144
	lin-41(ma104)	14	18	118	136
	psr-1(tm469)	25	16	48	64
	pmk-3(ok169)	0	0	56	56
	dlk-1(tm4024)	0	0	68	68
	ebp-1(tm1357)	0	0	64	64
	ced-7(n1996); let-7(mg279)	22	21	73	94
	eff-1(ok1021); let-7(mg 279)	24	17	55	72
	lin-41(ma104); let-7(mg279)	13	12	84	96
	let-7(mg279); shrEx11(P*mec-4 -let-7*)	31	28	62	90
	let-7(mg279); shrEx12(P*mec-4-let-7*)	39	34	52	86
	shrEx12(P*mec-4-let-7*)	18	16	73	89
	shrEx62(P*dpy-7-let-7*)	57	24	26	50
	shrEx59(P*mec-4-eff-1*-mCherry)	58	15	25	40
	eff-1(ok1021); *shrEx59*(P*mec-4-eff-1*-mCherry)	73	38	14	52
tbIs222 (P*mec-4*-mCherry)	Wild type	37	40	68	108
	let-7(mg279)	60	25	17	42

Table S2. Values of the relative change in mRNA levels (Ct) and fold change ($2^{-\Delta\Delta Ct}$) in qRT-PCR

Target gene	Mean ΔΔCt	ΔΔCt SEM	Fold modulation $2^{-\Delta\Delta Ct}$	Range
lin-41	0.9980	0.020	2.235	1.06–4.68
ced-7	0.5672	0.047	1.536	1.60–3.09
eff-1	0.0683	0.052	1.198	0.37–2.42
psr-1	0.0034	0.013	1.059	0.40–1.89

Table S3. Comparative values of GFP::RAB-3 particle flux during regeneration in control and *let-7(mg279)* worms at different ages

Stage	Fusion/no fusion	Position of ROI	Direction of movement	RAB-3 particle flux (no. particles·μm^{-1}·s^{-1}), mean ± SEM: Wild type	*let-7(mg279)*	*P* value
Before axotomy						
L4		30 μm from cell body	Anterograde	0.015 ± 0.0006	0.016 ± 0.0011	NS
			Retrograde	0.005 ± 0.0003	0.009 ± 0.0007	NS
A3			Anterograde	0.012 ± 0.0004	0.017 ± 0.0013	***
			Retrograde	0.0053 ± 0.0002	0.007 ± 0.0004	NS
Postaxotomy						
L4	Fusion	Distal	Anterograde	0.013 ± 0.001	0.011 ± 0.0009	NS
			Retrograde	0.007 ± 0.0010	0.005 ± 0.0001	NS
		Proximal	Anterograde	0.016 ± 0.0015	0.001 ± 0.001	NS
			Retrograde	0.0078 ± 0.0013	0.003 ± 0.0005	NS
	No fusion	Distal	Anterograde	0.0012 ± 0.0002	0.001 ± 0.0005	NS
			Retrograde	0.0011 ± 0.0004	0.0007 ± 0.0007	NS
		Proximal	Anterograde	0.010 ± 0.0011	0.004 ± 0.0015	NS
			Retrograde	0.006 ± 0.0008	0.001 ± 0.0005	NS
A3	Fusion	Distal	Anterograde	0.0023 ± 0.0004	0.0148 ± 0.0013	***
			Retrograde	0.00102 ± 0.0002	0.006 ± 0.0008	***
		Proximal	Anterograde	0.007 ± 0.0008	0.015 ± 0.0015	***
			Retrograde	0.0025 ± 0.0004	0.007 ± 0.0009	**

NS, not significant; *$P < 0.01$; **$P < 0.001$; ***$P < 0.0001$.

Table S4. Strains carrying newly generated extrachromosomal transgenes

Strain	Transgene	DNA construct	Genetic background	Concentration, ng/μl
NBR158	*shrEx11*	pNBRGWY16 (P*mec-4-let-7*)	*let-7(mg279); muIs32*	10
NBR159	*shrEx12*	pNBRGWY16 (P*mec-4-let-7*)	*let-7(mg279); muIs32*	10
NBR271	*shrEx12*	pNBRGWY16 (P*mec-4-let-7*)	*muIs32*	—
NBR273	*shrEx62*	pNBRGWY36 (P*dpy-7-let-7*)	*let-7(mg279); muIs32*	10
NBR267	*shrEx59*	pNBRGWY41 (P*mec-4-eff-1*-mCherry)	*muIs32*	20
NBR278	*shrEx59*	pNBRGWY41 (P*mec-4-eff-1*-mCherry)	*let-7(mg279); muIs32*	—
NBR263	*shrEx58*	pNBRGWY40 (P*mec-4-eff-1*-GFP)	*tbIs222*	20
NBR27	*shrEx71*	pNBRGWY38 (P*mec-4*-GFP with *ced-7* 3′ UTR)	*tbIs222*	10
NBR98	*shrEx71*	pNBRGWY38 (P*mec-4*-GFP with *ced-7* 3′ UTR)	*let7(mg279); tbIs222*	—
NBR28	*shrEx72*	pNBRGWY38 (P*mec-4*-GFP with *ced-7* 3′ UTR)	*tbIs222*	10
NBR70	*shrEx72*	pNBRGWY38 (P*mec-4*-GFP with *ced-7* 3′ UTR)	*let7(mg279); tbIs222*	—
NBR68	*shrEx72; shrEx12*	pNBRGWY38 (P*mec-4*-GFP with *ced-7* 3′ UTR), pNBRGWY16 (P*mec-4-let-7*)	*tbIs222*	—
NBR31	*shrEx73*	pNBRGWY43 (P*mec-4*-GFP with *ced-7* 3′ UTR LCS mutation)	*tbIs222*	10
NBR67	*shrEx74*	pNBRGWY43 (P*mec-4*-GFP with *ced-7* 3′ UTR LCS mutation)	*tbIs222*	10
NBR275	*shrEx59*	pNBRGWY41 (P*mec-4-eff-1*-mCherry)	*eff-1(ok1021); muIs32*	—

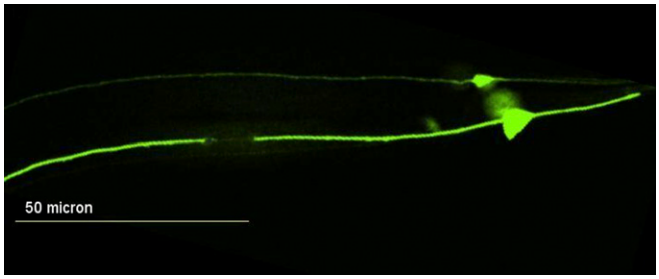

Movie S1. Axotomy of PLM neurons on both sides. The movie shows axotomy of PLMs on both the right and left sides using a 920-nm laser for scanning and a 720-nm laser for cutting. The axons were cut at ~50 μm from the cell body. Two cuts 6 μm apart were introduced on each side. The video was recorded using CamStudio Open Source software at a speed of two frames/s and is played four times faster.

Movie S1

Movie S2. Gentle touch response assay. The time-lapse movie shows the reversal behavior of a wild-type worm in response to an eyelash touch in the anterior and posterior parts at the L4 stage. The movie was recorded using a Leica MZ 10F modular stereomicroscope at 10× magnification fitted with a Leica MC 120 HD camera. The movie was captured at a speed of 10 frames/s using SkyStudioPro software and is played at the same speed.

Movie S2

Movie S3. Loss of posterior touch response after axotomy. The time-lapse movie shows the gentle touch response assay 10 h after axotomy of PLM neurons on both sides. Note that worm is specifically impaired in posterior touch response. The movie was recorded as describe for Movie S2 at a speed of 29 frames/s and is played at the same speed.

Movie S3

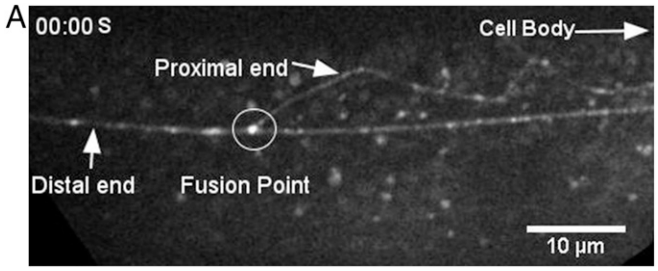

Movie S4*A*. Time-lapse movie depicting Rab-3 trafficking in a T2 fusion event after axotomy at stage L4. The movie was captured using a spinning-disk confocal microscope at 100× magnification with an EMCCD camera. The movie was captured at a speed of three frames/s and is played five times faster. The positions of the cell body and proximal and distal ends are marked.

Movie S4*A*

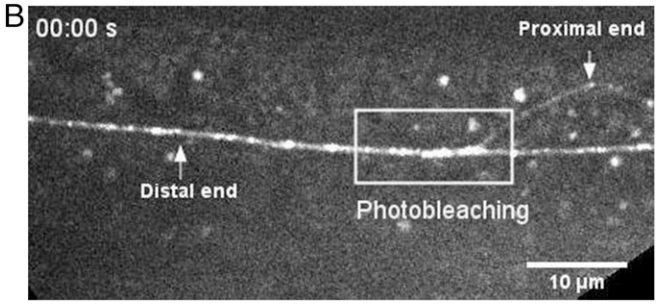

Movie S4*B*. Time-lapse movie depicting RAB-3 trafficking in a fusion event as shown in Movie 4*A* after photobleaching. The movie was captured using a spinning-disk confocal microscope at 100× magnification with an EMCCD camera. The movie was captured at a speed of three frames/s and is played five times faster. The positions of the cell body and proximal and distal ends are marked.

Movie S4*B*

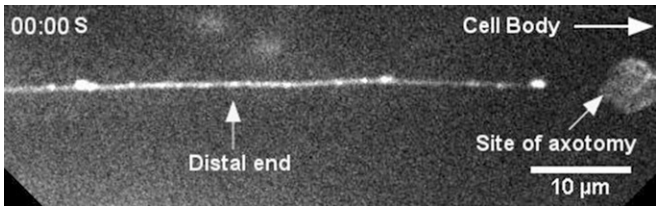

Movie S5. Time-lapse movie depicting Rab-3 trafficking in the distal end in a nonfusion event after axotomy at the L4 stage. The movie was captured using spinning-disk confocal microscope at 100× magnification with an EMCCD camera. The movie was captured at a speed of three frames/s per and is played five times faster. The positions of the cell body and distal end are marked.

Movie S5

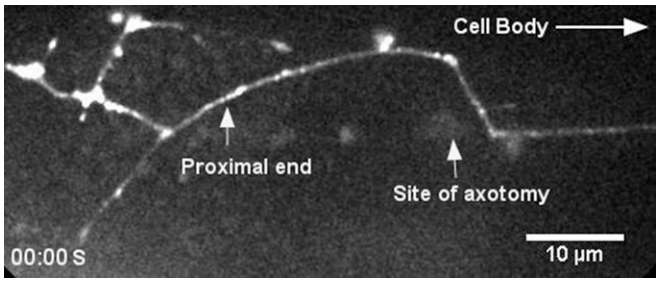

Movie S6. Time-lapse movie depicting Rab-3 trafficking in a regrowing proximal end in a nonfusion event after axotomy at the L4 stage. The movie was captured using a spinning-disk confocal microscope at 100× magnification with an EMCCD camera. The movie was captured at a speed of three frames/s and is played five times faster. The positions of the cell body and proximal end are marked.

Movie S6

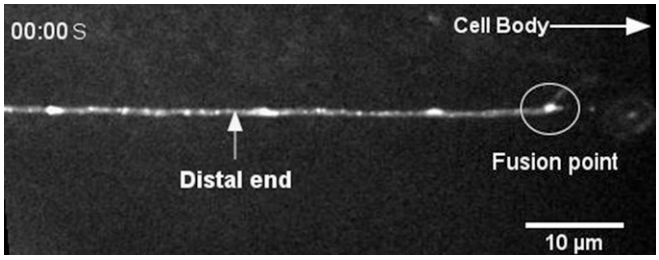

Movie S7. Time-lapse movie depicting Rab-3 trafficking at the distal end in a fusion event after axotomy at the L3 stage in a wild-type control worm. The movie was captured using a spinning-disk confocal microscope at 100× magnification with an EMCCD camera. The movie was captured at a speed of three frames/s and is played five times faster. The positions of the cell body and distal end are marked.

Movie S7

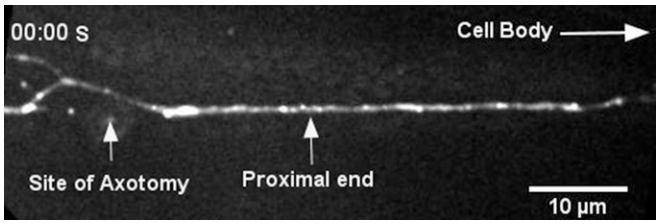

Movie S8. Time-lapse movie depicting Rab-3 trafficking at the proximal end in a fusion event after axotomy at the A3 stage in a wild-type control worm. The movie was captured using a spinning-disk confocal microscope at 100× magnification with an EMCCD camera. The movie was captured at a speed of three frames/s and is played five times faster. The positions of the cell body and proximal end are marked.

Movie S8

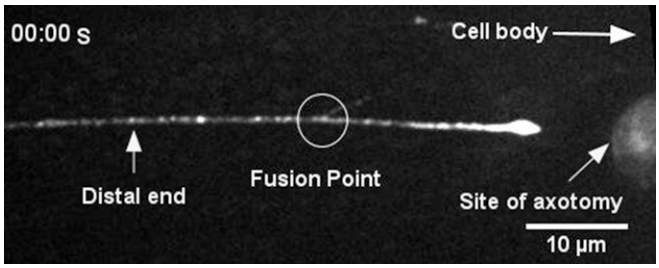

Movie S9. Time-lapse movie depicting Rab-3 trafficking at the distal end in a fusion event after axotomy at the A3 stage in a *let-7(lf)* worm. The movie was captured using a spinning-disk confocal microscope at 100× magnification with an EMCCD camera. The movie was captured at a speed of three frames/s and is played five times faster. The positions of the cell body and distal end are marked.

Movie S9

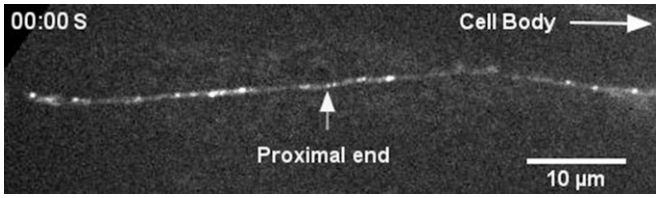

Movie S10. Time-lapse movie depicting Rab-3 trafficking at the proximal end in a fusion event after axotomy at the A3 stage in a *let-7(lf)* worm. The movie was captured using a spinning-disk confocal microscope at 100× magnification with an EMCCD camera. The movie was captured at a speed of three frames/s and is played five times faster. The positions of the cell body and proximal end are marked.

Movie S10